ADVANCED INTELLIGENT SYSTEMS
Open Access
www.advintellsyst.com

Magnetic Hair Tactile Sensor for Directional Pressure Detection

*Yuki A. Meier, Pierre Duhr, Marcel Mordarski, Céline Vergne, Erik Poloni, André R. Studart, Joris Pascal, and Ahmet F. Demirörs**

Tactile sensing in the human body is achieved via the skin. This has inspired the fabrication of synthetic skins with pressure sensors for potential applications in robotics, bio-medicine, and human–machine interfaces. Tactile sensors based on magnetic elements are promising as they provide high sensitivity and a wide dynamic range. However, current magnetic tactile sensors mostly detect pressures of solid objects and operate at relatively high forces about 100 mN. Herein, these limitations are addressed by manufacturing soft, stretchable, and hair-like structures that are permanently magnetized to achieve high-resolution, cost-effective, and high-resolution pressure sensing. Combining these hair-like structures with advances in 3D magnetic-field measurements allows us to monitor directional tactile pressures without solid contact. To prove the concept of this technology, a bio-inspired soft device is built with a hairy structure that senses and reports environmental mechanical stresses, similar to that of human skin. Simple self-assembly of the soft magnetic hair structure makes our approach easy to scale for large-area applications.

1. Introduction

Touch is one of the most important senses, as it allows us to extract object properties such as shape, hardness, texture, and temperature[1,2] via interactions and explorations. This high amount of information is perceived within various layers of human skin[3] by various types of receptors such as mechanoreceptors (pressure), thermoreceptors (temperature), and nociceptors (pain and damage). For instance, human hands have a high density of mechanoreceptors accurately providing tactile information.[4] Creating synthetic versions of such sensors is of great technological interest due to their applications in prosthetics,[5] robotics,[6] automation,[7] human–machine interactions,[8,9] and health monitoring.[10]

Although tactile sensors are becoming increasingly used in daily life, from traffic lights to safety belt alarms in vehicles, they are still far away from providing the complex functions, softness, and resolution of the *human skin*. One promising way of fabricating tactile sensors is based on magnetic elements, which provide high sensitivity, wide dynamic range, robustness,[7] and even contactless sensing[11] in some cases. However, current magnetic tactile sensors are mostly limited to 2D sensing,[12] suffer from low resolution,[13] and require expensive permanent magnets for operation.[14] Even advanced magnetic tactile sensors still lack the detection resolution of fingertips, which can detect features down to 1 mm.

In this work, these restrictions are addressed by manufacturing soft, stretchable, and hair-like structures that carry a permanent magnetic moment for high-resolution and cost-effective pressure sensing. Directional tactile sensing is achieved by measuring changes in the 3D magnetic field resulting from physical interactions with the environment. This enabled the fabrication of a novel bio-inspired device that reports stresses born of solids or gases. Soft magnetic hair (MagHair) sensors exhibit an exceptional resolution of 700 μN and have a working range of 0–20 mN. Thus, they combine high resolution, airflow sensing, and self-assembly fabrication with force field mapping which enables shape detection.

2. Results

The device is composed of two parts (**Figure 1**). The first part consists of a soft magnetic carpet, which is a composite soft matrix with short magnetic hairs on top.[15,16] The composite and the hairs contain magnetic particles with a preexisting dipole moment (i.e., magnetic memory) with an orientation along the

Y. A. Meier, P. Duhr, M. Mordarski, E. Poloni, A. R. Studart, A. F. Demirörs
Complex Materials, Department of Materials
ETH Zurich
8093 Zurich, Switzerland
E-mail: ahmet.demiroers@unifr.ch

C. Vergne, J. Pascal
Institute for Medical Engineering and Medical Informatics, School of Life Sciences
FHNW Muttenz
4132 Muttenz, Switzerland

A. F. Demirörs
Department of Physics
University of Fribourg
CH-1700 Fribourg, Switzerland

The ORCID identification number(s) for the author(s) of this article can be found under https://doi.org/10.1002/aisy.202400106.

DOI: 10.1002/aisy.202400106

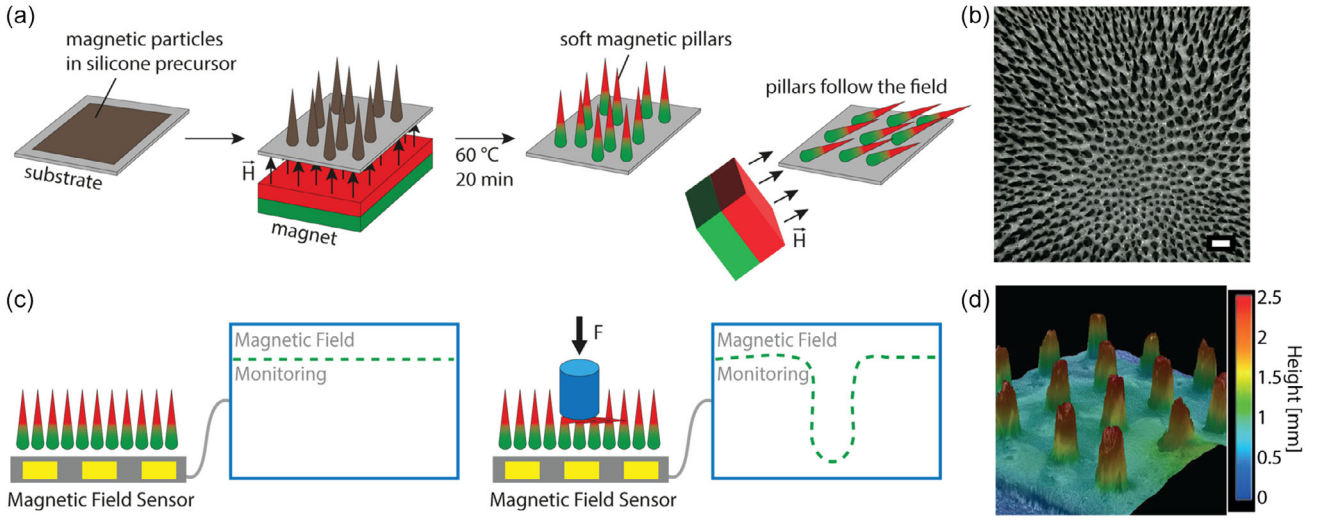

Figure 1. Fabrication and working principle of the soft magnetic pressure sensor. a) Sketch of the soft magnetic hairy (MagHair) sensor fabrication with NdFeB powder and a silicone precursor. b) Top view of a typical sample used for pressure monitoring. Scale bar: 100 µm. c) The working principle of the soft pressure sensor that detects the applied pressure based on magnetic field deviations of the permanently magnetized soft hairy film. d) A reflection microscopy 3D scan of the MagHair sensor surface with the height profile.

hair. Due to this directionality, the magnetic field induces changes in response to applied mechanical forces. The second part of the device is a triaxial magnetic field sensor[17,18] arranged in a soft matrix or an array of magnetic field sensors. They spatially detect and map the magnetic field alterations over the soft magnetic carpet. Detection of the magnetic field changes by an array of sensors under the soft magnetic carpet provides information about the location, direction, and magnitude of the applied forces.

The ability to monitor the direction of the applied stresses stems from the anisotropic shape and magnetization of the hairs and the wide spectrum of the triaxial magnetic field detector. The angle detection for applied stresses is rare[12] and can be instrumental to measure lateral stresses and shear forces.[12] Moreover, manufacturing a device with such a hairy design enables the fabrication of soft but durable tactile sensors with high sensitivity to forces even in the absence of hard contact. This imbues a device with enhanced sensing capabilities, including the ability to measure the pressure of a blowing gas.

The magnetized hair structures are created by embedding hard magnetic particles in a polymer matrix followed by curing in the presence of a magnetic field to induce the alignment of particles (dipoles) and thus enhance the magnetic moment of the composite. Due to the high volume fraction of magnetic particles, the hair-like pillars display a strong magnetic moment that enables self-assembly driven by the Rosensweig instability.[19] Such an assembled structure provides a significant magnetic moment to be detected in response to mechanical forces. In addition, it allows for a soft hairy surface that detects gentle forces without hard contact to the matrix.

An array of soft pillars that exhibit a permanent magnetization was fabricated by modifying a previously reported procedure[15,16,19,20] (see Methods). In brief, a mixture of neodymium iron boron (NdFeB) particles (Magnequench MQFP-B+, D50 ≈25 µm) and a soft silicone matrix (Ecoflex 00-20) was first spread on a supporting substrate (Figure 1a). To this layer, a homogeneous magnetic field was applied perpendicular to the substrate during the course of the polymerization. This caused the spontaneous formation of pillars due to a Rosensweig-type instability.[20] An example of the produced MagHair sensor can be seen in micrographs in Figure 1b,d. Usefully, the size and density of the pillar array can be tuned by changing the applied field strength, the magnetic particle content, and the total amount of the magnetic mixture.[15,16]

Once fully polymerized, the pillars respond to external magnetic fields. This is a consequence of the permanent magnetic dipole moment of the pillars. Such dipole moments are generated by the homogeneous external field applied during fabrication, which aligns the moments of the individual NdFeB particles present in the composite. When an external field is applied parallel to the dipole moment of the pillars, they stand and stretch along the field lines. When the magnetic field is oppositely directed, it bends the pillars onto the substrate surface.

The response of the MagHair sensor to magnetic fields is reversible over many cycles. Less intuitively but still usefully, an external mechanical force that deflects the otherwise standing pillars causes a local magnetic field response. This is because the soft pillars possess a permanent magnetic dipole and their deflection results in a magnetic field variation. The magnetic field changes are significant enough to be detected by state-of-the-art magnetic field sensors[17,21] (Figure 1c). Indeed, a three-dimensional magnetic field sensor detects the field changes in all axes and can therefore be used for pressure detection in three dimensions. These features can be combined to fabricate a magnetic tactile sensor with superior sensitivity to the human skin.

To quantify the resolution and performance of the magnetic tactile sensor, the effect of applied forces on changes in the detected magnetic field is measured (**Figure 2**). When a specific pressure is applied, the magnetic field flux over the MagHair sensor changes in response. This response allowed us to detect and

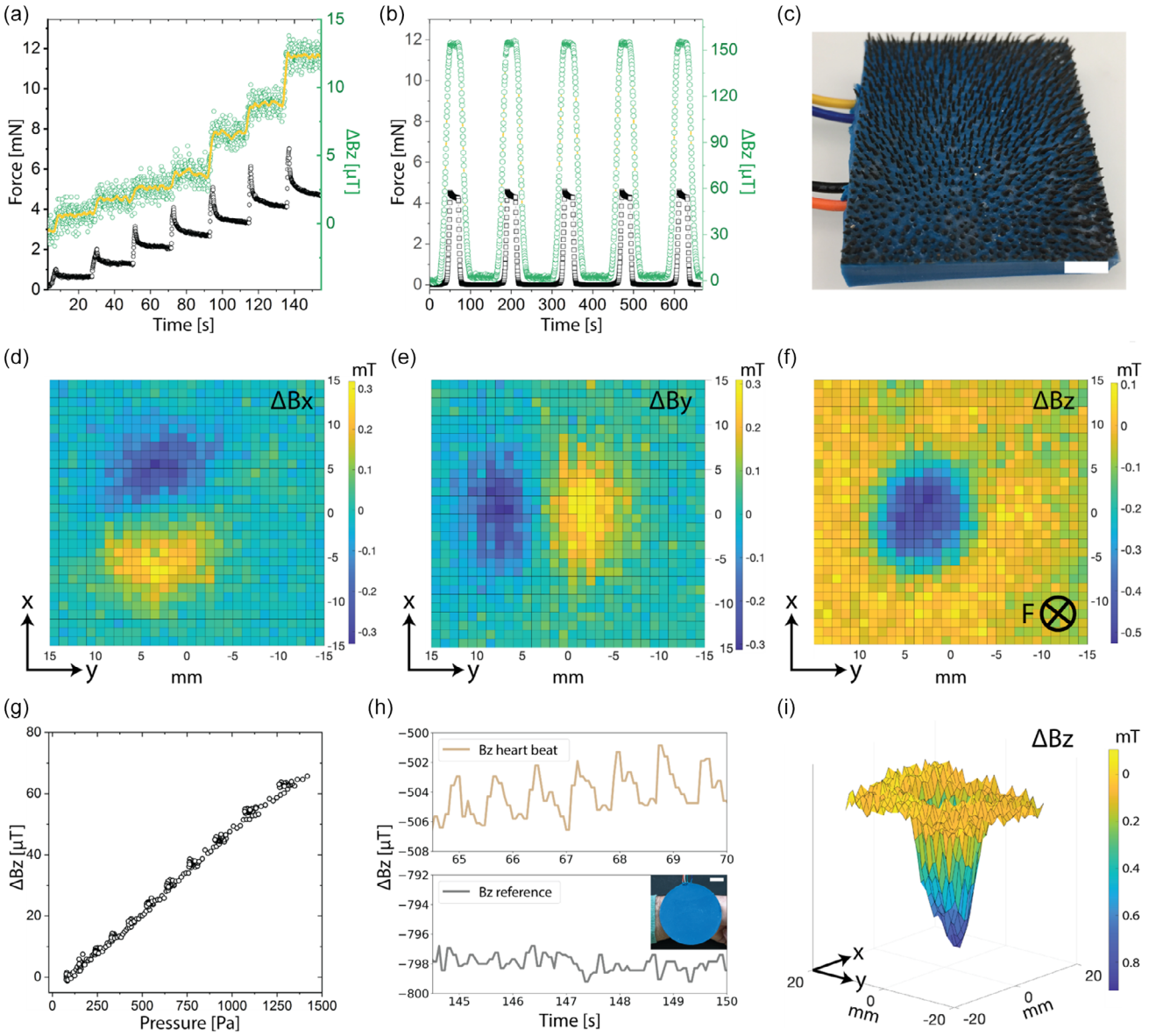

Figure 2. Magnetic field response of the MagHair sensor to applied forces. a) Applied force (left) and corresponding magnetic field response in the *z*-axis ΔB_z (right) as a function of time. The yellow curve was obtained by averaging the data for ΔB_z. b) Force cycles applied on the MagHair sensor show the reversibility of the magnetic response generated. c) Photograph of the soft sensor with magnetic hairs. Scale bar: 5 mm. d–f) Magnetic field response detected along the d) *x*-, e) *y*-, and f) *z*-axes to a 9.8×10^{-3} N (867 Pa) force orthogonally applied to the MagHair sensor surface. F in the inset shows the direction of the applied force. g) Calibration of the magnitude of the magnetic field changes against the applied pressures. h) Heartbeat oscillations of an author detected by the MagHair sensor (top) and control data (bottom) containing fluctuations detected by the idle sensor. The inset shows a photo of the setup. Scale bar: 1 cm. i) Side view of the plot in (f), illustrating the depth profile of the magnetic field changes along the *z*-axis when a force is applied orthogonal to the sensor surface.

report forces in the mN range. Force measurements were performed with a mechanical tester (Shimadzu AGX) with predefined 0.1 mm displacements. The forces acting on the 1 cm diameter disc probe were measured during these probe-displacement steps. Simultaneously, the corresponding changes in the magnetic field along the *z*-axis, ΔB_z, were recorded. Due to the alignment of the pillar's magnetic moment along the *z*-axis, the most significant magnetic field changes were anticipated to occur along the *z*-axis.

Remarkably, the MagHair sensor setup was able to capture and resolve displacement events even at forces as low as ≈0.7 mN (Figure 2a–c and Figure S1, Supporting Information), which corresponds to a pressure of ≈10 Pa. This is an order of magnitude lower than the human skin sensing resolution, which is reported to be 100–300 Pa.[22] The change in the magnitude of the force and magnetic response in time observed in Figure 2a is due to the displacement control of the setup (see Experimental Section) and the conical shape of the magnetic pillars. For both

force and magnetic response, when the force sensor displaces the tip of the cone, it is expected that less volume is deflected compared to the middle and bottom of the cone. Therefore, the applied force and the magnetic response increase through the constant displacement steps. Although we have used the magnetic field response along the z-axis, ΔB_z, to demonstrate the force detection capabilities of the MagHair sensor, the x- and y-components of the magnetic field also see appreciable changes in response to applied forces. To monitor these magnetic field changes, we mapped a 30 mm × 30 mm area with an array of magnetic field sensors that measure the x, y, and z components of the field 2.5 mm under the MagHair sensor. When a pressure of 870 Pa was applied orthogonal to the MagHair sensor surface (in the z-axis), noticeable changes in the x, y, and z components of the magnetic field were detected (Figure 2d–f). The field changes in the x and y axes show maxima and minima polarized along the orthogonal axes, which evidences the soft pillars bending in a radially symmetric fashion (Figure 2d,e). Such homogenous bending of the soft pillars causes a superior depression in the magnetic field along the z-axis (Figure 2f,i, see also Figure S2 (Supporting Information) for the force vectors).

To use the MagHair setup as a force sensor, we performed controlled experiments to correlate the applied pressure with magnetic field changes. These measurements resulted in a linear calibration curve of the ΔB_z with respect to the applied pressure (Figure 2g). Such linear response is observed up to a pressure of ≈1500 Pa, after which a plateau is achieved as the reversible bending limit for the pillar is reached. To illustrate the high resolution of the sensor, we measured the heart pulses of an author in the radial artery between the wrist bone and the tendon on the thumb side of the wrist. The oscillations of the heartbeats are detectable by the sensor when compared to a control sample left idle (Figure 2h). Using a single magnetic field sensor, it is possible to detect the stress applied to the MagHair sensor. Moreover, we foresee that using multiple magnetic field sensors may allow us to obtain spatial information and thereby detect local applied stress and the shape of the touching object.

To demonstrate the shape-detection capabilities of the MagHair sensors, we measured the magnetic field changes induced by placing objects of distinct geometries on the surface of the magnetic carpet. An array of magnetic sensors enabled real-time monitoring of the magnetic field changes under the MagHair sensor during the experiment. With spatial magnetic field information, the MagHair sensor setup was able to detect the shape of the object pressing the soft hairs. A solid object with a flat face or a surface with a topography is easily identifiable by this method. Indeed, our experiments reveal that different shapes pressed over the MagHair sensor resulted in magnetic field changes that matched the geometry of the objects (**Figure 3**). Flat-faced objects such as stars, discs, or cubes lead to magnetic field changes with a corresponding flat pattern (Figure 3a–c). Furthermore, shapes such as a ring, a triangular prism with a frame, or a snowman (Figure 3d–f) were easily captured. Note that in the triangular prism, the ≈1 mm height difference of the frame (the edges are thicker than the center with 1 mm profile depth) was also detected in the measurement (Figure 3e).

In addition to shape recognition of solid objects, the MagHair sensors can also operate in a contactless mode to detect the magnitude and the direction of forces applied by gases blown on the carpet surface. We illustrate these capabilities by measuring the magnetic field changes when a gas is blown at different angles on the MagHair sensor surface. First, the air was blown orthogonal

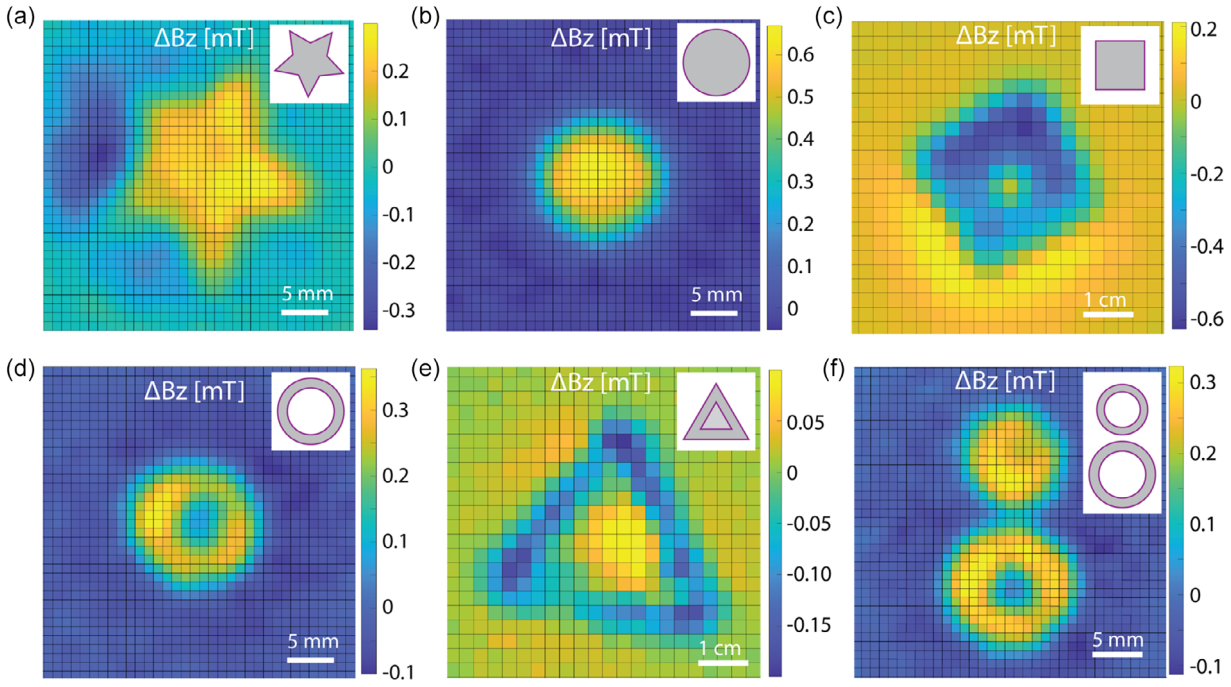

Figure 3. Shape detection using MagHair sensors with an array of magnetic field sensors. Differently shaped objects were pressed on the MagHair sensor, and the shape of the object was detected with the magnetic field reading. Magnetic field readings are shown for a) a star, b) a disc, c) a cube, d) a ring, e) a triangle with a frame, and f) snowman-shaped objects.

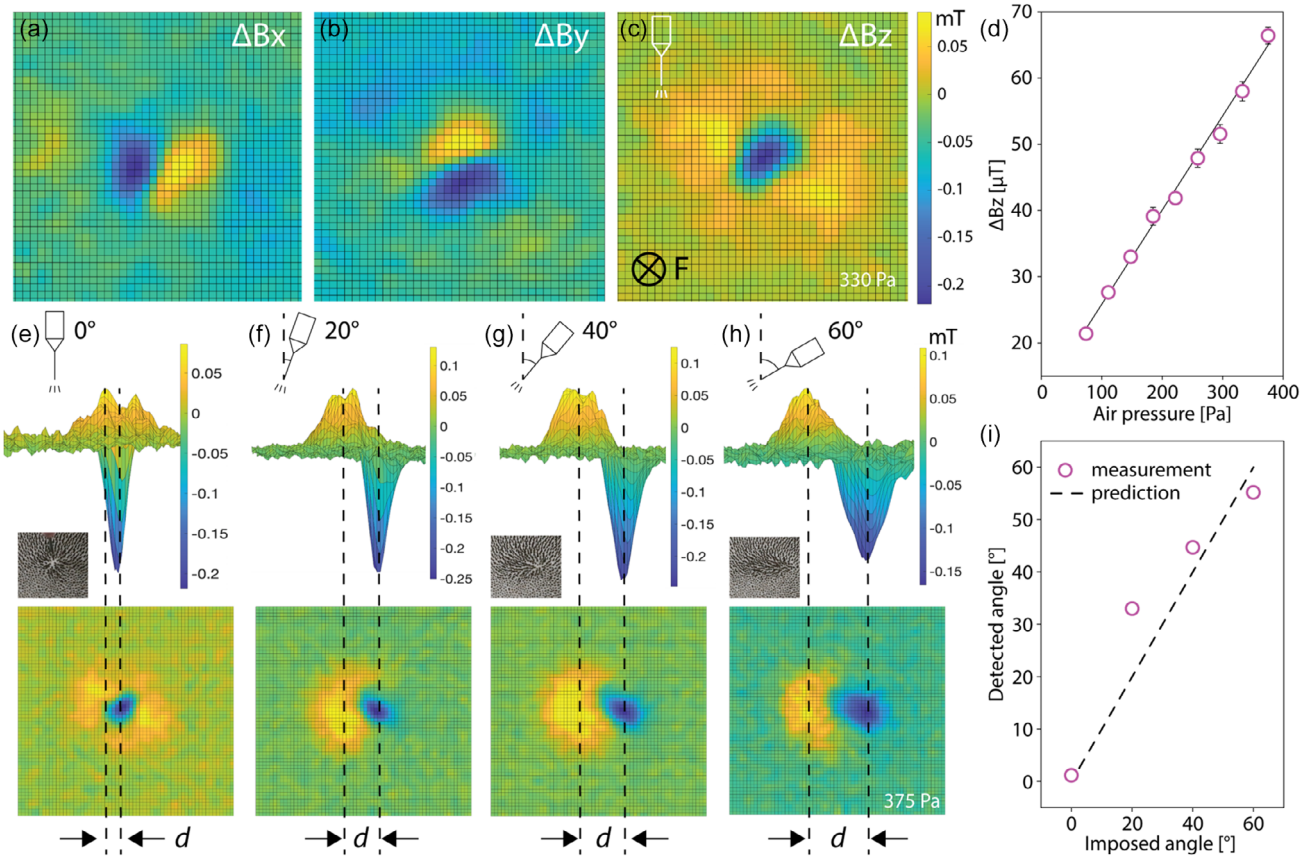

Figure 4. Sensing the air blow pressure with angle detection. a–c) Magnetic field changes on a MagHair sensor for an air blow angle of $\theta = 0$ measured in a) *x*-axis, a) *y*-axis, c) *z*-axis. d) Calibration of the air blow pressures against the magnetic field changes in *z*, ΔB_z. e–h) Dependence of the magnetic field readings to the angle of the blown air. The top panels show the side view of the magnetic field changes, which demonstrates the evolution of a minimum and a maximum with a nonorthogonal gas blow. The bottom panels show the top view (*xy* plane) of the magnetic field changes with the varying angle of the nozzle tip that blows at an angle from $\theta = 0°$ to $\theta = 60°$. Insets show a photo showing the physical changes over the MagHair sensor. The physical distance between the maximum and the minimum over the *y*-axis increases with an increasing angle, and it is shown for the different angles. Note that the angle changes are performed in the *yz*-plane. i) The known angles of the experiments in (e–h) are compared with the predicted angles from the magnetic field measurements.

to the surface of the sensor at varying pressures through a nozzle with 0.53 mm inner diameter. For an arbitrary air pressure of 375 Pa and nozzle-to-surface distance of 17 mm, the magnetic field changes over the mapped area were similar to the ones observed with a solid probe (**Figure 4**a–c, see also Figure S3 (Supporting Information) for the force vectors). The field changes in the x and y axes show maxima and minima polarized along orthogonal axes similar to a solid probe (Figure 2a,b). To correlate the magnetic field changes with the applied air pressure, we increased the applied pressure from 75 to 375 Pa while recording the respective magnetic field changes. These measurements revealed a linear dependence of ΔB_z with respect to the applied air pressure (Figure 4d). Such linear response is observed up to a pressure of ≈375 Pa, which was the upper limit of the pressurized air available in our measurement setup.

When the direction of the air pressure is shifted by a given tilt angle θ in the *yz* plane, a clear change is observed in the distribution of the hair bending and the respective magnetic field reading (Figure 4e–h inset). Starting from a tilt angle $\theta = 20°$, a maximum and a minimum emerged in the magnetic field map of ΔB_z (Figure 4e–h). They are not observed for the ΔB_z reading when the tilt angle was $\theta = 0°$. Instead, a tilt angle $\theta = 0°$ leads only to a minimum peak, which is surrounded by a circular area of slightly increased field around the minima (Figure 4f). This increased circular ring is less clear for lower air pressures. When θ is increased from $\theta = 20°$ to $\theta = 60°$, the maximum and minimum peaks are retained and the minimum peak is elongated and shifted along the tilt direction (Figure 4f,h). Such observable changes in the magnetic field maps in the *z*-axis allow us to predict the angle of the applied air pressure. For this, we quantified the relative peak shift by measuring the distance *d* between the minima and maxima locations. Using simple trigonometry, we estimated the angle θ by taking the inverse tangent (*arctan*) of the ratio of the distance *d* to the height of the nozzle relative to the MagHair sensor surface. Our experiments show that this relation can be used to predict the angle of the applied air pressure (Figure 4i). We believe that further exploration of this concept can give access to shear forces in tactile sensing platforms, which is a desired property in current robotics.[12,23,24]

3. Theoretical Background

Although the soft pillars experience both compression and buckling due to their anisotropy and softness, the buckling effect dominates. We assume a buckling beam model with the first mode[25,26] for the compression of the soft pillars. Following the Euler–Bernoulli force and moment balance[25,26] for an elastic beam, the stress changes linearly with the strain which scales as $\sigma_b \approx 2\sigma_c\left(\Delta L/L\right)$ where σ_b is the stress for buckling, $\Delta L/L$ is the relative displacement, and σ_c is the critical minimal stress for buckling. Thus, the applied stress changes linearly against $\Delta L/L$.

To compute changes in the magnetic field of soft pillars along the z-axis, we consider that the z component of the magnetic field can be written as the sum of the contribution of each infinitesimally small section of the pillar. Based on this approach, the magnetic field strength scales with $\Delta L/L$ and is given by $B_z = B_{zi}\left(1 - \Delta L/L\right)$, where B_{zi} is the initial magnetic field in the z-axis and B_z is the magnetic field in z after buckling. Consequently, changes in magnetic field can be expressed as $\Delta B_z = B_{zi} - B_z \approx B_{zi}\left(\Delta L/L\right)$ (**Figure 5**). Here it is observed that the change of ΔB_z has a linear response to the $\Delta L/L$. Because both ΔB_z and σ scale with $\Delta L/L$, the relationship between ΔB_z and σ should be linear, as demonstrated in experimental Figures 2g and 4d.

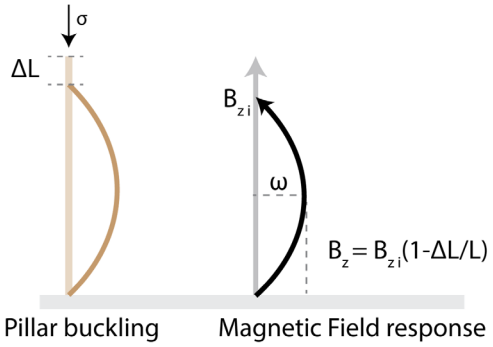

Figure 5. Sketch showing the soft pillar bending and its relation to the displacement and the magnetic field response.

4. Discussion

The state of the art for tactile sensors using magnetic sensors and magnetic elements for force detection is presented in **Table 1**. The table compares the fabrication, magnetic element (magnet, magnetic film, or cilia), resolution, range, capabilities to detect air blow, 3D forces and to perform mapping (enable e.g., shape detection) aspects. The comparison shows that the permanent magnets and films have a higher working range but exhibit lower resolution to smaller forces. Therefore, they cannot detect air flows. The early demonstrations of magnetic cilia have improved resolution compared to permanent magnets that are comparable to our work, and these sensors have lower working force ranges. Ribeiro et al.[27] reported magnetic cilia consisting of 5 pillars and observed the possibility of sensing air blow but without further investigation. Directional force sensing and mapping were not shown in these studies.[27–29] Man et al.[30] reported on casted magnetic cilia with superior resolution and airflow detection with a lower detection range, as a result of the high field magnetization and the high aspect ratio of the cilia. Therefore, we believe that the aspect ratio of the cilia can be suggested as a parameter to tune the sensor resolution depending on the application. Our work combines higher resolution, airflow sensing, and self-assembly methods with additional force field mapping demonstrations enabling shape detection. From a manufacturing point of view, the self-assembly methods in our work are easier and allow for the possibility to scale up.

5. Conclusions

A soft and stretchable magnetic carpet fitted with hair-like structures was manufactured and used for high-resolution, angle-sensitive pressure sensing based on magnetic field measurements. The permanent magnetic moment of the hair-like soft carpet was instrumental in detecting the pressure applied to

Table 1. Comparison of the state-of-the-art tactile sensors based on magnetic sensors and elements.

Work	Methodology (cilia, film, or magnet)	Fabrication mthod	Resolution	Range	Airflow detection	3D force sensing	Force field mapping
Youcan[12]	Multiple films	Manual	10 mN	0–10 N	No	Yes	Yes
Mohammadi[14]	Permanent magnet	Casting	1.5 N	1.5–10 N	No	No	Yes
Wang[31]	Permanent magnet	Casting	5 mN	0–1.5 N	No	Yes	No
Dwivedi[32]			1.2 mN	3.3 N	No	Yes	No
Hellebrekers[13]	Magnetic film	Casting	0.25 N	0.14–2.4 N	No	No	Yes
Ribeiro et al[27]	Magnetic cilia	Casting	333 µN	0–26 mN	Sensing[a)]	No	No
Alfadhel[28]	Magnetic cilia	Casting	6 mN	55 mN	No	No	No
Man[30]	Magnetic cilia	Casting	2.1 µN	60 µN	Yes	Yes	No
Man[33]	Magnetic cilia	Casting	0.2 mN	19.5 mN	No	Yes	No
Virta[29]	Magnetic cilia	Self-assembly	–	–	No	No	No
MagHair	Magnetic cilia	Self-assembly	700 µN	0–20 mN	Yes	Yes	Yes

[a)]No calibration and force measurements were demonstrated. Only the response of the sensor to the blow was shown.

these structures. In addition to the highly sensitive detection of pressure from solid probes, the hairy design of the sensor also enables the contactless quantification of gas pressures. By blowing air onto the MagHair sensor surface and recording the magnetic field changes, we obtained magnetic field maps that can also be used to sense the directionality of the applied air pressure. In contrast to many tactile sensing technologies based on piezo effects and capacitance changes, the MagHair sensors reported here do not require direct contact, making it a suitable alternative for applications related to gas pressure detection. In future research, the stiffness of the hairs and the magnetic content of the hairs can be adjusted to address prescribed mechanical loads or deformations. This enables tuning the range of the detectable forces to the requirements of specific applications. In addition, the flexible shape of the MagHair sensor can be potentially modified to conform to the geometry or topology of a potential host system. We anticipate applications of MagHair sensor setup in soft robotics, medical devices, and human–machine interfaces as a competitive tactile sensor, especially when cost-effective but highly sensitive force measurements are needed.

6. Experimental Section

Fabrication of the MagHair Sensor: We modified a previously reported method[19,20] to fabricate our soft, magnetic pillars. First, we prepared a mixture of Ecoflex 00-20 (a platinum-catalyzed silicone rubber compound, Smooth-on Inc.), hexane (Sigma Aldrich, ACS reagent), and magnetic neodymium iron boron particles (NdFeB, Magnequench MQFP-B+, D50 = ≈25 μm, 10215-088, Lot #F00492) with a weight ratio of 4:1:x, where *x* corresponds to the NdFeB particle concentration. In a typical experiment, we added 4 g of Ecoflex (2 g of each component), 1 g of hexane, and 3.6 g of NdFeB powder (44 wt%). This mixture was homogenized in a Thinky mixer (ARE-250) for 3 min at 2000 rpm. Next, 1 g of this mixture was poured into a Teflon petri dish (3 cm × 3 cm, 0.25 mm thickness) and spread evenly by moving a permanent magnet (NdFeB, www.supermagnete.ch) back and forth underneath the Petri dish, touching its bottom. Typically, the magnet had a dimension of 5 cm × 5 cm × 2 cm and a strength of 0.4 T. We could make pillars with different lengths and shapes by varying the strength of the magnet and the amount of the mixture used. Once pillars were formed, we increased the spacing between the magnet and the Petri dish by 0.5 cm and moved this to an oven to be cured for 20 min at 60 °C, which solidified the silicone matrix (i.e., Ecoflex 00-20). The distance between the magnet and the petri dish was deliberately chosen to be 0.5 cm because this distance is a practical optimum for a high and homogeneous field above the permanent magnet.

To fabricate cilia arrays with consistent length, several parameters were kept identical. The magnet and its magnetic field (distance to the substrate) were kept unchanged. In addition, the amount of the magnetic spread in weight and thickness was kept the same for all the samples. Besides these parameters, the uniformity of the cilia sizes over a surface also depended on the size of the permanent magnet used. With a 5 cm × 5 cm area magnet, we were able to obtain uniform assemblies of 3.5 cm × 3.5 cm soft magnetic pillars. This is due to the field strength distribution over the magnet which is different in the middle and the edge of the magnet.

Magnetometer and MagHair Sensor Assembly: The magnetic hairy elastomer was peeled from the preparation cup and glued on top of the commercial magnetic field sensor board (LSM303AGR; Adafruit) by using a minimal amount of Ecoflex 00-20 mixture. After the curing, the magnetic hairy carpet was fixed on the sensor board. The commercial magnetic field sensor was embedded in a stiffer silicone (Zhermack Silicone ZA 50, TrollFactory) with a 2.5 mm distance to the magnetic sensing unit. The MagHair sensor required proximity for the magnetic flux changes to be detected, but no electrical connection to the underlying magnetometer board was necessary. To avoid the undesired effect of the Earth's magnetic field on the measurements, we took the magnetic field difference ΔBz and kept the orientation of the setup unchanged with respect to the Earth's field.

For the mapping experiments, a magnetic field mapper (Hallinsight; Metrolab SA) with 32 × 32 tri-axis Hall sensors on a 75 mm × 75 mm area was placed under the soft magnetic carpet for simultaneous recording of the field changes over an area of interest. Note that the use of two different magnetic sensor technologies reveals different sensitivities and measurements in solid-contact (Figure 2d) and air-blow (Figure 4d) experiments. Besides the sensor technology, the distance of the magnetic pillars to the sensing unit (Hallinsight mapper distance was 2 mm and for the LSM303AGR sensor 2.5 mm) also changes the readings. All sensor measurements were performed at room temperature.

Air Pressure Experiments and Angle Prediction: A tube with pressurized air at 5 bar was connected to a syringe to apply air pressure on the MagHair sensor surface at different tilt angles. The syringe needle served as the pressure nozzle. This setup resulted in air pressures on the surface of the MagHair sensor from 75 to 375 Pa. The syringe tip had a flat cut and had an inner diameter of 0.53 mm. The tip was fixed to a lab stand, and the tilt angle was adjusted by a triangular ruler to a fixed angle θ of 0°, 20°, 40°, or 60°. The prediction of the angle θ_{est} was performed by the following simple formula $\theta_{est} = \arctan\left(\frac{d}{h_{nozzle}}\right)$ where d is the distance between the maxima and the minima in the ΔB_z map, and h_{nozzle} is the height of the nozzle tip from the surface of the MagHair sensor. The pressure applied on the MagHair sensor was also calibrated by using a laboratory scale to inspect the forces applied.

Mechanical Force Measurements and Sensor Resolution: Force measurements were performed with a mechanical tester (Shimadzu AGX) using a 10 N load cell, which had a minimal force resolution of about ≈3 mN. Tests were performed in the compression mode and with a displacement control of 100 μm steps by using a disc probe with a diameter of 1 cm. To minimize any magnetic interference, we used plastic 3D-printed discs as the probe with a minimum 2 cm distance to any metallic unit . To assess the resolution of the force sensor, we divide the range of successful measurements by the number of detections shown in Figure 2a. This results in the 0.7 mN resolution.

Supporting Information

Supporting Information is available from the Wiley Online Library or from the author.

Acknowledgements

The authors thank ETH Zürich for the financial support of this research. This research was partially supported by the Swiss National Science Foundation through the National Centre of Competence in Research Bio-Inspired Materials (grant number: 51NF40_182881).

Conflict of Interest

The authors declare no conflict of interest.

Data Availability Statement

The data that support the findings of this study are available at 10.5281/zenodo.11390931 and from the corresponding author upon reasonable request.

Keywords

magnetic fields, pressure sensor, self-assembly, soft materials, tactile sensor

Received: February 7, 2024
Revised: May 6, 2024
Published online: June 12, 2024

[1] S. J. Lederman, R. L. Klatzky, *Cognit. Psychol.* **1987**, *19*, 342.
[2] X. Wang, L. Dong, H. Zhang, R. Yu, C. Pan, Z. L. Wang, *Adv. Sci.* **2015**, *2*, 1500169.
[3] R. S. Johansson, G. Westling, *Exp. Brain Res.* **1984**, *56*, 550.
[4] A. B. Vallbo, R. Johansson, *Hum. Neurobiol.* **1984**, *3*, 3.
[5] R. I. Ponder, M. Safaei, S. R. Anton, *J. Mech. Behav. Biomed. Mater.* **2019**, *91*, 237.
[6] R. L. Truby, M. Wehner, A. K. Grosskopf, D. M. Vogt, S. G. M. Uzel, R. J. Wood, J. A. Lewis, *Adv. Mater.* **2018**, *30*, 1706383.
[7] P. S. Girão, P. M. P. Ramos, O. Postolache, J. Miguel Dias Pereira, *Measurement* **2013**, *46*, 1257.
[8] Y. Lu, D. Kong, G. Yang, R. Wang, G. Pang, H. Luo, H. Yang, K. Xu, *Adv. Sci.* **2023**, *10*, 2303949.
[9] D. Kong, G. Yang, G. Pang, Z. Ye, H. Lv, Z. Yu, F. Wang, X. V. Wang, K. Xu, H. Yang, *Adv. Intell. Syst.* **2022**, *4*, 2200050.
[10] A. D. Valentine, T. A. Busbee, J. W. Boley, J. R. Raney, A. Chortos, A. Kotikian, J. D. Berrigan, M. F. Durstock, J. A. Lewis, *Adv. Mater.* **2017**, *29*, 1703817.
[11] J. Ge, X. Wang, M. Drack, O. Volkov, M. Liang, G. S. Cañón Bermúdez, R. Illing, C. Wang, S. Zhou, J. Fassbender, M. Kaltenbrunner, D. Makarov, *Nat. Commun.* **2019**, *10*, 4405.
[12] Y. Yan, Z. Hu, Z. Yang, W. Yuan, C. Song, J. Pan, Y. Shen, *Sci. Robot.* **2021**, *6*, abc8801.
[13] T. Hellebrekers, O. Kroemer, C. Majidi, *Adv. Intell. Syst.* **2019**, *1*, 1900025.
[14] A. Mohammadi, Y. Xu, Y. Tan, P. Choong, D. Oetomo, *Sensors* **2019**, *19*, 4925.
[15] A. F. Demirörs, S. Aykut, S. Ganzeboom, Y. A. Meier, E. Poloni, *Proc. Natl. Acad. Sci.* **2021**, *118*, e2111291118.
[16] A. F. Demirörs, S. Aykut, S. Ganzeboom, Y. A. Meier, R. Hardeman, J. de Graaf, A. J. T. M. Mathijssen, E. Poloni, J. A. Carpenter, C. Ünlü, D. Zenhäusern, *Adv. Sci.* **2021**, *8*, 2102510.
[17] T. Quirin, C. Féry, D. Vogel, C. Vergne, M. Sarracanie, N. Salameh, M. Madec, S. Hemm, L. Hébrard, J. Pascal, *Sensors* **2021**, *21*, 2670.
[18] C. Vergne, J. Inácio, T. Quirin, D. Sargent, M. Madec, J. Pascal, *IEEE Sens. J.* **2023**, *24*, 7336.
[19] H. Lu, M. Zhang, Y. Yang, Q. Huang, T. Fukuda, Z. Wang, Y. Shen, *Nat. Commun.* **2018**, *9*, 3944.
[20] J. V. I. Timonen, C. Johans, K. Kontturi, A. Walther, O. Ikkala, R. H. A. Ras, *ACS Appl. Mater. Interfaces* **2010**, *2*, 2226.
[21] P. Badertscher, C. Vergne, C. Féry, D. Mannhart, T. Quirin, S. Osswald, M. Kühne, C. Sticherling, S. Knecht, J. Pascal, *IJC Heart Vasc.* **2022**, *43*, 101122.
[22] T. Xu, W. Wang, X. Bian, X. Wang, X. Wang, J. K. Luo, S. Dong, *Sci. Rep.* **2015**, *5*, 12997.
[23] W. Yuan, R. Li, M. A. Srinivasan, E. H. Adelson, in *2015 IEEE Inter. Conf. on Robotics and Automation (ICRA)*, IEEE, Piscataway, NJ **2015**, pp. 304–311, https://doi.org/10.1109/ICRA.2015.7139016.
[24] D. Gueorguiev, J. Lambert, J.-L. Thonnard, K. J. Kuchenbecker, *Sci. Rep.* **2022**, *12*, 8215.
[25] S. P. Timoshenko, J. M. Gere, *Theory of Elastic Stability*, Courier Corporation, Mineola, New York **2012**.
[26] J. J. Lugthart, Buckling of a Beam The Force-Engineering Strain Curve. Batchelor Thesis, Leiden University, Leiden **2013**. https://www.universiteitleiden.nl/binaries/content/assets/science/mi/scripties/bachlugthart.pdf.
[27] P. Ribeiro, M. A. Khan, A. Alfadhel, J. Kosel, F. Franco, S. Cardoso, A. Bernardino, J. Santos-Victor, L. Jamone, *IEEE Trans. Magn.* **2017**, *53*, 1.
[28] A. Alfadhel, M. A. Khan, S. Cardoso de Freitas, J. Kosel, *IEEE Sens. J.* **2016**, *16*, 8700.
[29] A. Virta, J. V. I. Timonen, R. H. A. Ras, Q. Zhou, in *2012 IEEE/RSJ Inter. Conf. on Intelligent Robots and Systems*, IEEE, Vilamoura-Algarve, Portugal **2012**, pp. 1–6, https://doi.org/10.1109/IROS.2012.6385623.
[30] J. Man, J. Zhang, G. Chen, N. Xue, J. Chen, *Microsyst. Nanoeng.* **2023**, *9*, 12.
[31] H. Wang, G. De Boer, J. Kow, A. Alazmani, M. Ghajari, R. Hewson, P. Culmer, *Sensors* **2016**, *16*, 1356.
[32] A. Dwivedi, A. Ramakrishnan, A. Reddy, K. Patel, S. Ozel, C. D. Onal, *IEEE Sens. J.* **2018**, *18*, 3852.
[33] J. Man, Z. Jin, J. Chen, *Adv. Sci.* **2024**, *11*, 2306832.